Experimental and simulation study of an air gap membrane distillation module with solar absorption function for desalination

H. Chang*, C.-L. Chang, C.-D. Ho, C.-C. Li, P.-H. Wang

Energy and Opto-Electronic Materials Research Center, Department of Chemical and Materials Engineering, Tamkang University, 151 Ying-Chuan Rd., Tamsui, Taipei County, Taiwan
Tel. +886 (2) 2623 2094; Fax +886 (2) 2620 9887; email: nhchang@mail.tku.edu.tw

ABSTRACT

Being capable of directly utilizing solar thermal energy, the solar driven membrane distillation desalination system has evolved as a promising technology for alleviating the energy and water resource problems. An innovative device for desalination, which is a hybrid of a solar collector and a membrane distillation, called SAF–AGMD (air gap membrane distillation with solar absorption function) is proposed. The experimental and simulation results are reported. The experimental results validate the feasibility of the design and the water production rate is enhanced by 2–8% compared to the simple AGMD module. The mathematic model takes into account the heat and mass transfers via correlations from the literature. The model is verified by the experimental data under different conditions, including the temperature and flow rate of inlet fluids, the air gap thickness and the solar radiation. The differences between the model predication and the experimental results are within 10%. The model is further incorporated with the experimental design method and response surface method for the optimization study. Considering water production and exergy loss, the optimal operation should use hot fluid of 325 K, cold fluid of 298 K and air gap thickness of 1.9 mm.

Keywords: Air gap membrane distillation; Desalination; Modeling; Optimization; Solar energy

1. Introduction

Membrane distillation (MD) is a thermally driven separation process, in which only vapor molecules are transported through porous hydrophobic membranes. The driving force is the vapor pressure difference between the hot liquid feed side and the cold permeate side of the membrane. MD systems can be classified into four configurations according to the nature of the cold side of the membrane, i.e. direct contact (DCMD), air gap (AGMD), sweeping gas (SGMD), and vacuum (VMD). The principles, applications and developments of MD have been comprehensively reviewed by several researchers [1–3].

One important application of MD is desalination, for example, Obaidani et al. [4] reported the integration of MD with the conventional pressure-driven membrane technology and crystallization for improving the performance of the overall system and the achieving the zero liquid discharge goal. Murase et al. [5] developed a hybrid desalination unit by combining the solar distillator and the membrane distillation for enhancing the water productivity.

Compared to other desalination technologies, the MD desalination system is highly competitive mainly due to

_____

* Corresponding author.

its low operating cost by using the low grade thermal energy. The solar driven MD desalination system, where energy is supplied entirely by flat-plate solar thermal collectors and photovoltaic panels, has been experimentally demonstrated by several research institutions [6–8] to be feasible and energetically competitive with other desalination processes. On the modeling and control of the solar powered desalination processes, Ben Bacha et al. [9] and Roca et al. [10] presented studies for a solar multiple condensation evaporation cycle system and a hybrid solar–fossil fuel powered multieffect distillation system, respectively. Dynamic modeling and control system for a solar driven membrane distillation desalination system, include solar collector, heat storage tank, heat exchanger and spiral wound AGMD modules, has been developed [11].

In the reported solar driven MD systems for desalination, the solar thermal energy is utilized to heat the feed stream of MD indirectly, i.e. via the heat exchange between the thermal storage fluid and the MD feed stream. In this study, an innovative device for desalination, which is a hybrid of a solar collector and an AGMD, called SAF–AGMD (air gap membrane distillation with solar absorption function) is proposed, as shown in Fig. 1.

The paper presents the experimental and simulation study for a SAF–AGMD module using flat membrane. The mathematical model is verified by experimental results and used for analyzing the effects of the operating variables and determining the optimal operating conditions.

2. Methods

2.1. Experimental

The experimental setup is illustrated in Fig. 2. The major experimental equipments include a set of solar simulator and a flat plate type AGMD module with solar absorption function. The solar simulator consists of 8 lamps with adjustable irradiance by a transformer.
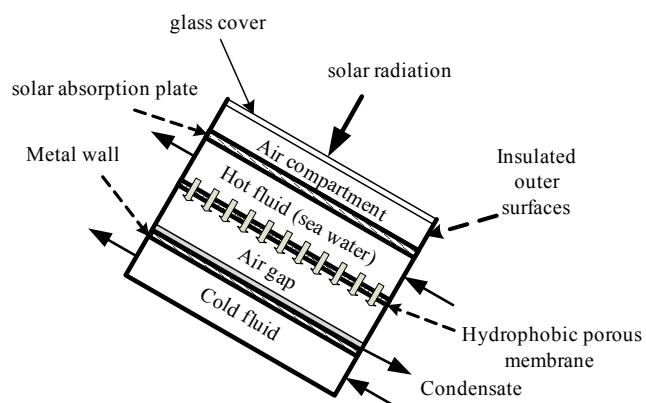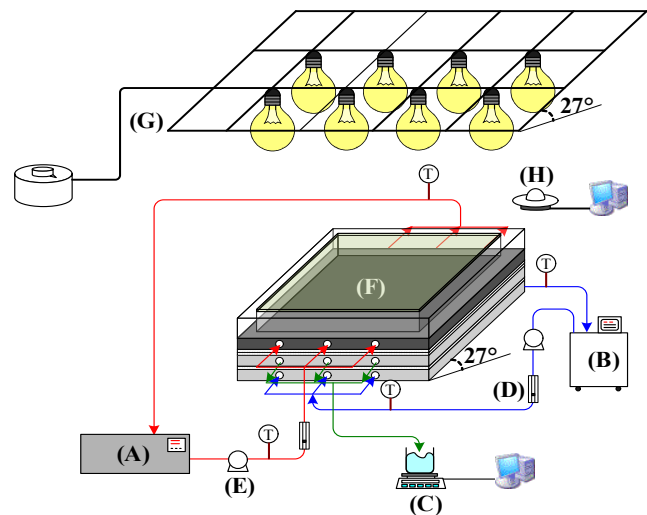

Fig. 1. SAF–AGMD module.

Fig. 2. Experimental setup for SAF–AGMD. (A) Hot fluid thermostat, (B) Cold fluid thermostat, (C) Beaker and electronic balance, (D) Flow meter, (E) Pump, (F) Membrane distillation module, (G) Transformer and infrared lamps, (H) Pyranometer.

The coated solar absorber plate is placed on top of the AGMD module. Under the absorber plate is the sea water to be heated which is the hot fluid to the AGDM and above the absorber plate is an air compartment enclosed by the plate and a glass cover. The system is insulated on all outer surfaces except the glass side to prevent the heat loss to the environment. The specifications of the experimental setup are listed in Table 1. The hot fluid is an aqueous solution of 3.5 wt% sodium chloride and the cold fluid is pure water. The module is tilted by an angle of 27° to the horizon for easy collection of the condensate and both fluids flow upward to ensure complete filling of the flow channels.

The solar irradiance received on top of the absorber plate is determined using a pyranometer (Model PSP, Eppley Laboratory, Inc.). For the hot fluid and cold fluid entering the AGMD module, the temperatures are controlled by thermostats. The condensate, which is the water transported through the membrane, is collected and measured for its temperature and flow rate with a thermocouple sensor and an electronic balance. The same experimental setup is also used for conducting the conventional AGMD experiments by taking away the solar absorption function. For the operation conditions implemented, the water production using SAF–AGMD is enhanced by 2–8% compared to AGMD.

2.2. Modeling

The 1D AGMD model reported in a published paper by the authors for the hollow fiber module [12] is modified for the flat plate type SAF–AGMD. The mass and energy fluxes for all layers, including the glass cover, air compart-

Table 1
Specifications of the experimental setup

Fixed parameters		Variable parameters	
Air compartment thickness, m	0.02	Solar radiation intensity, W/m^2	830, 1100
Area of solar absorption plate, m^2	0.05	Air gap thickness, mm	1.9, 4
Length of flow channel, m	0.25	Flow rate of hot fluid, L/min	0.3–0.9
Width of flow channel, m	0.2	Inlet temperature of hot fluid, K	313–328
Height of flow channel, mm	2	Flow rate of cold fluid, L/min	0.3–0.9
Metal plate thickness	0.01 m (aluminum)	Inlet temperature of cold fluid, K	288–298
Material of membrane	Composite membrane of PTFE and PP (ADVANTEC)		
Membrane thickness, μm	130		
Membrane pore diameter, μm	0.2		
Membrane porosity	0.74		
Membrane tortuosity	1.35		

ment (referred as air gap 1), absorption plate, hot fluid, membrane, air gap (referred as air gap 2), condensing liquid, metal plate and cold fluid, are illustrated in Fig. 3. The model equations are summarized in Table 2. In the model, the mass transfer flux is determined by considering the mass transfer resistances in the membrane and air gap 2, because the resistances of the hot fluid side, cold fluid side and condensing liquid are insignificant [12]. With its small flow rate, the condensate film is very thin and the heat transfer resistance is neglected. The heat transfer resistances of all other layers are taken into account.

The heat and mass transfer coefficients needed in the model are calculated using the equations listed in Table 3.

For the air gap 1 and air gap 2, the Rayleigh numbers are estimated to be about 8,000 and 10, respectively. Hence, for the air gap 2, only heat conduction is taken into account. On the other hand, the heat transfer coefficient of the air gap 1 is estimated using the correlation for free convection in an inclined enclosure by Hollands et al. [13]. For the hot fluid and cold fluid, because L/D_e is greater than Re/20, the entrance effect can be neglected [14]. The heat transfer coefficients are hence estimated using the solution for fully developed laminar flow forced convection
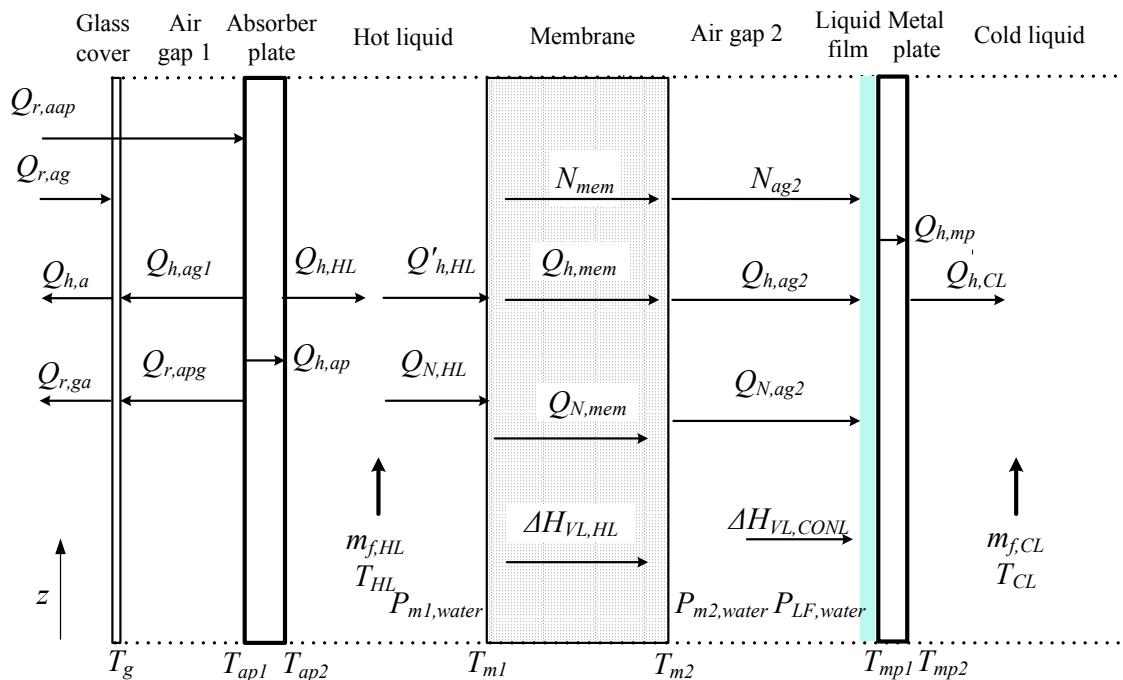

Fig. 3. Heat and mass transfers in SAF–AGMD module.

Table 2
Model equations for SAF–AGMD

Mass balances		Heat fluxes	
$\dfrac{dm_{f,HL}}{dz} = N_{mem} Mw_{water} W$	(1)	$Q_{h,a} = h_a (T_g - T_a)$	(15)
$\dfrac{dm_{f,CONL}}{dz} = -N_{ag2} Mw_{water} W$	(2)	$Q_{r,ga} = \left[1/(1/e_g + 1/e_a - 1) \right] \sigma (T_g^4 - T_a^4)$	(16)
$N_{mem} = N_{ag2}$	(3)	$Q_{r,ag} = \alpha_g I(t)$	(17)
Energy balances		$Q_{r,aap} = \tau_g \alpha_{ap} I(t)$	(18)
$\dfrac{m_{f,HL}}{M_{HL}} \dfrac{\partial T_{HL}}{\partial z} = \dfrac{W}{M_{HL} C_{p,HL}^L} \left(Q_{h,HL} - Q'_{h.HL} - Q_{N,HL} \right)$	(4)	$Q_{h,ag1} = h_{ag1} \left(T_{ap1} - T_g \right)$	(19)
$\dfrac{m_{f,CL}}{M_{CL}} \dfrac{\partial T_{CL}}{\partial z} = \dfrac{W}{M_{CL} C_{p,CL}^L} Q_{h,CL}$	(5)	$Q_{r,apg} = \left[1/(1/e_{ap} + 1/e_g - 1) \right] \sigma \left(T_{ap1}^4 - T_g^4 \right)$	(20)
$Q_{r,ag} + Q_{h,ag1} + Q_{r,apg} = Q_{h,a} + Q_{r,ga}$	(6)	$Q_{h,ap} = h_{ap} \left(T_{ap1} - T_{ap2} \right)$	(21)
$Q_{r,aap} = Q_{h,ag1} + Q_{r,apg} + Q_{h,ap}$	(7)	$Q_{h,HL} = h_{HL} \left(T_{ap2} - T_{HL} \right)$	(22)
$Q_{h,ap} = Q_{h,HL}$	(8)	$Q'_{h,HL} = h_{HL} \left(T_{HL} - T_{m1} \right)$	(23)
$Q'_{h,HL} + Q_{N,HL} - \Delta H_{VL,HL} = Q_{h,mem} + Q_{N,mem}$	(9)	$Q_{N,HL} = N_{mem} C_{p,HL}^L \left(T_{HL} - T_{m1} \right)$	(24)
$Q_{h,mem} + Q_{N,mem} = Q_{h,ag2} + Q_{N,ag2}$	(10)	$\Delta H_{VL,HL} = N_{mem} \Delta H_{vap,m1}$	(25)
$Q_{h,ag2} + Q_{N,ag2} + \Delta H_{VL,CONL} = Q_{h,mp}$	(11)	$Q_{h,mem} = h_{mem} \left(T_{m1} - T_{m2} \right)$	(26)
$Q_{h,mp} = Q_{h,CL}$	(12)	$Q_{N,mem} = N_{mem} C_{p,mem}^V \left(T_{m1} - T_{m2} \right)$	(27)
Mass fluxes		$Q_{h,ag2} = h_{ag2} \left(T_{m2} - T_{mp1} \right)$	(28)
$N_{mem} = \dfrac{k_{mem}}{R \overline{T}_E} \left(P_{m1,water} - P_{m2,water} \right)$	(13)	$Q_{N,ag2} = N_{ag2} C_{p,ag2}^V \left(T_{m2} - T_{mp1} \right)$	(29)
$N_{ag2} = \dfrac{k_{ag2} P_{system}}{R \overline{T}_{ag2} P_{\ln,ag2}} \left(P_{m2,water} - P_{LF,water} \right)$	(14)	$\Delta H_{VL,CONL} = N_{ag2} \Delta H_{vap,mp1}$	(30)
		$Q_{h,mp} = h_{mp} \left(T_{mp1} - T_{mp2} \right)$	(31)
		$Q_{h,CL} = h_{CL} \left(T_{mp2} - T_{CL} \right)$	(32)

in rectangular channels with the boundary condition of constant wall temperature [15]. For the absorption plate, membrane and metal plate, the thermal conductivities and thicknesses of these materials are used for calculating the heat transfer coefficients. The heat transfer coefficient of the ambient air is assumed to be a constant of 4.8 W/m^2 K. In Eq. (36), the thermal conductivity of membrane (K_{mem}) is computed as the volume average of the vapor conductivity and the solid polymer membrane conductivity. Other thermally related properties, which

are assumed constant, include the thermal conductivities, the heat capacities, the heat of vaporization, the emissivities of the glass and the absorption plate (0.94 and 0.039), the effective heat penetration coefficient of the glass (0.88) and the effective absorptivity of the absorption plate (0.9).

For the mass transfer in the porous membrane, Knudsen diffusion and molecular diffusion are taken into account via the resistance-in-series approach as shown in Eq. (39). For the air gap 2 with a thickness of only several mm, the mass transfer coefficient is estimated from the

Table 3
Estimation of transfer coefficients

Coefficient	Equation	
Heat transfer coefficient of air gap 1 (h_{ag1})	$\mathrm{Nu}_{ag1} = 1 + 1.44 \left[1 - \dfrac{1708}{Ra_{ag1} \cos \phi} \right]\left[1 - \dfrac{1708 \sin (1.8\phi)^{1.6}}{Ra_{ag1} \cos \phi} \right] + \left[\left(\dfrac{Ra_{ag1} \cos \phi}{5830} \right)^{\frac{1}{3}} - 1 \right]$	(33)
Heat transfer coefficient of absorption plate (h_{ap})	$h_{ap} = \dfrac{K_{ap}}{\delta_{ap}}$	(34)
Heat transfer coefficient of hot liquid (h_{HL}) and cold liquid (h_{CL})	$\mathrm{Nu} = 7.541$	(35)
Heat transfer coefficient of membrane (h_{mem})	$h_{mem} = \dfrac{K_{mem}}{\delta_{mem}}$	(36)
Heat transfer coefficient of air gap 2 (h_{ag2})	$h_{ag2} = \dfrac{K_{ag2}}{\delta_{ag2}}$	(37)
Heat transfer coefficient of metal plate (h_{mp})	$h_{mp} = \dfrac{K_{mp}}{\delta_{mp}}$	(38)
Mass transfer coefficient of membrane (k_{mem})	$k_{mem} = \dfrac{\varepsilon}{\tau} \left[\dfrac{1}{1/D_k + y_{air,\ln}/D_m} \right] \dfrac{1}{\delta_{mem}}$	(39)
Mass transfer coefficient of air gap 2 (k_{ag2})	$k_{ag2} = \dfrac{D_m}{\delta_{ag2}}$	(40)

diffusivity of water vapor in air by Eq. (40). The Knudsen diffusivity is calculated using Eqs. (6.5–14) in [16]. The molecular diffusivities are estimated by the empirical equation of Fuller et al. [17].

3. Results and discussion

3.1. Model validation

The model is verified by comparing the simulation results with the experimental results under the operating conditions listed in Table 1. The differences between the model predictions and the experimental results are less than 10%. The results of varying the thickness of air gap 2, the solar intensity, and the temperature and flow rate of hot fluid are shown in Fig. 4.

3.2. Effects of operating variables

The effects of operating variables on the performances of SAF–AGMD are analyzed using the model and the results are summarized in Table 4. The performance index analyzed include the water flux (N), exergy loss (Ex_{Loss}), and thermal efficiency (η). The exergy loss is the differ-

ence between the inlet exergy, from solar radiation and inlet streams, and the outlet exergy, from outlet streams. The concept of exergy analysis is referred to Bejan [18]. The thermal efficiency is defined as the ratio of the total energy input to the system used for phase change. The results indicate that the variables which lead to significant effects are the hot fluid temperature, cold fluid temperature and thickness of air gap 2.

3.3. Optimization

For the three significant operating variables, T_{HL}, T_{CL}, and δ_{ag2}, the optimization study is accomplished using the model. Because the performance index of exergy loss and thermal efficiency are similar in their meanings, the objective function is defined by considering the water flux (N) and the exergy loss (Ex_{Loss}) as:

$$f = N / N_{ref} - Ex_{Loss} / Ex_{Loss,ref} \qquad (41)$$

where both N and Ex_{Loss} are normalized by a specified reference value. For the optimization analysis, a surrogate function of the objective function and the three decision variables is developed first. The surrogate function is
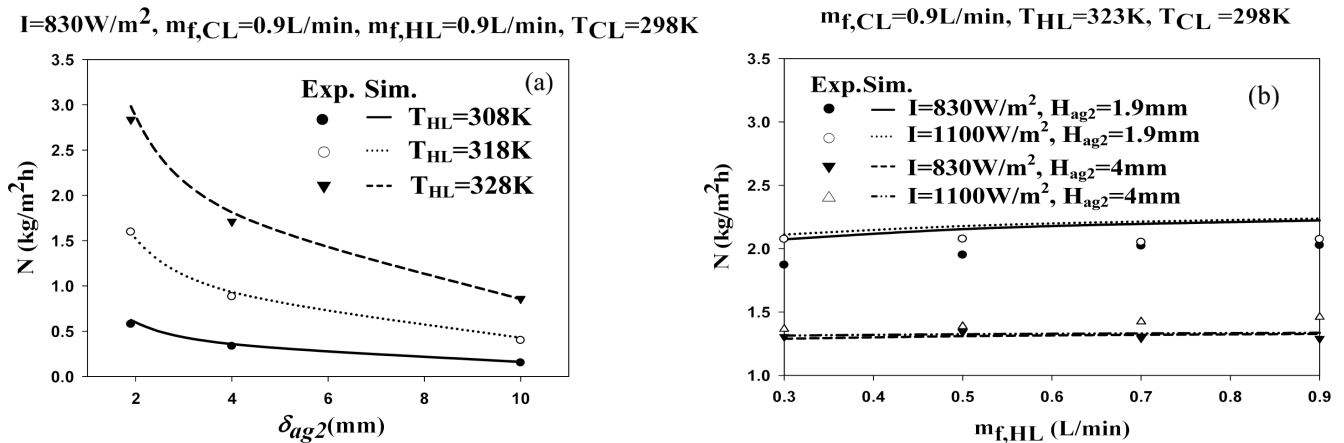
I=830W/m², m$_{f,CL}$=0.9L/min, m$_{f,HL}$=0.9L/min, T$_{CL}$=298K

m$_{f,CL}$=0.9L/min, T$_{HL}$=323K, T$_{CL}$ =298K

Fig. 4. Comparisons of simulation and experimental results for SAF–AGMD.

determined by the response surface method (RSM) [19] with a second-order polynomial function as Eq. (42):

$$f = \beta_0 + \beta_1 T_{HL} + \beta_2 T_{CL} + \beta_3 \delta_{ag2} + \beta_4 T_{HL}^2 + \beta_5 T_{CL}^2 + \beta_6 \delta_{ag2}^2$$
$$+ \beta_7 T_{HL} T_{CL} + \beta_8 T_{HL} \delta_{ag2} + \beta_9 T_{CL} \delta_{ag2} \quad (42)$$

The coefficients (β) of the polynomial function are determined by the method of multiple linear regression based on the data points selected using the design of experiment (DOE) method, the Latin hypercube design (LHD) method [20]. With 50% excess data points, 15 data points are determined and simulated by the mathematical model for the performance of the SAF–AGMD. The comparison of the objective function values from the model simulation and from the surrogate function, as shown in Fig. 5, demonstrates the applicability of the surrogate function.

The optimization search is then implemented on the surrogate function to maximize the objective function. The ranges of the decision variables for the study are 313–328 K for T_{HL}, 288–298 K for T_{CL}, and 1.9–10 mm for δ_{ag2}. The optimal operation should use 325 K for T_{HL}, 298 K for T_{CL}, and 1.9 mm for δ_{ag2}. The corresponding

performances are water flux of 2.524 kg/m²h, exergy loss of 7.86 J/s, and thermal efficiency of 0.8653. The results concluded that the key variable that influences the trade-off between the water flux and the exergy loss is the temperature of hot fluid and the optimal value is not at the highest temperature, on the other hand, for the other two variables, the lowest temperature of cold fluid and the smallest thickness of air gap 2 should be adopted.
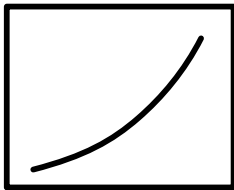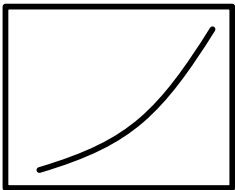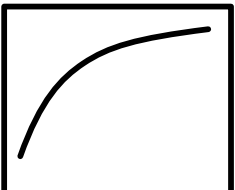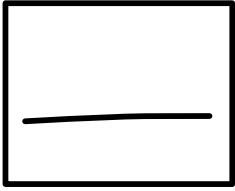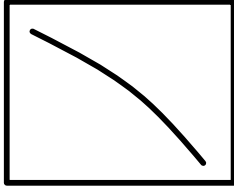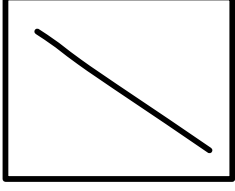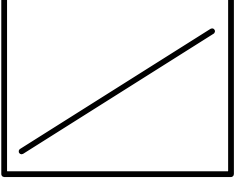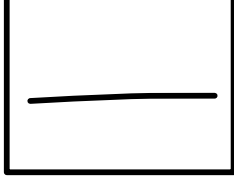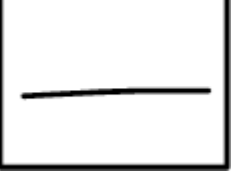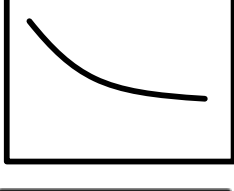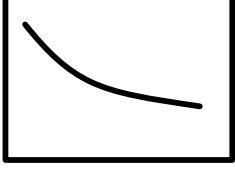
4. Conclusions

The innovative SAF–AGMD (air gap membrane distillation with solar absorption function) for desalination has been investigated by both experimental and modeling approaches. The experimental results show an increase of 2–8% in water production by the solar absorption function. The mathematical model developed considers the heat and mass transfer of each layer of the module. The operating variable study and optimization analysis reveal that the important variables are the hot fluid temperature, cold fluid temperature, and the air gap thickness. However, the key var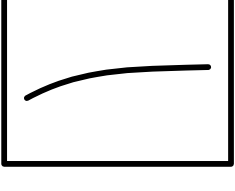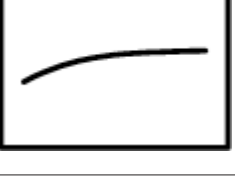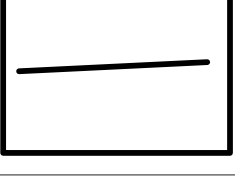iable that influences the trade-off of the two performance index, water flux and exergy loss, is the hot fluid temperature and an optimal temperature should be used. For the other two variables, the highest cold fluid temperature and the smallest air gap thickness should be used. Further study should be focused on how to increase the area of the solar absorber that can be employed on the SAF–AGMD in order to obtain greater enhancement in water production.

Symbols

C_p	—	Heat capacity, J/kg K
D	—	Diffusivity, m²/s
D_e	—	Hydraulic diameter, m
D_m	—	Molecular diffusivity, m²/s
D_k	—	Knudsen diffusivity, m²/s

Fig. 5. Comparison of simulation and regression results.

Table 4
Effects of operating variables

Operating variable (x-axis)	Performance index (y-axis)		
	N (kg/m² h)	Ex_{Loss} (J/s)	η_t
T_{HL} (K)			
$m_{f,HL}$ (L/min)			
T_{CL} (K)			
$m_{f,CL}$ (L/min)			
δ_{ag2} (mm)			
I (W/m²)			

e	—	Emissivity	
Ex	—	Exergy, J/s	
h	—	Heat transfer coefficient, W/m² K	
I	—	Intensity of solar radiation, W/m²	
k	—	Mass transfer coefficient, m/s	
K	—	Thermal conductivity, W/m K	
L	—	Length of the module, m	
M	—	Mass of the hot or cold fluid in the module, kg	
M_w	—	Molecular weight of water, kg/kmol	
m_f	—	Mass flow rate, kg/s	
N	—	Mole flux of water, kmol/m² s	
Nu	—	Nusselt number	

P	—	Pressure, Pa
Q_h	—	Heat transfer rate by convection or conduction, J/s
Q_N	—	Heat transfer rate by the temperature change of the water flux, J/s
Q_r	—	Heat transfer rate by radiation, J/s
R	—	Gas constant, Pa m³/kmol K
Ra	—	Rayleigh number
Re	—	Reynolds number
T	—	Temperature, K
$\bar{T}$	—	Average temperature, K
W	—	Width of the module, m

Greek

α	—	Effective absorptivity
β	—	Coefficient of the polynomial function
ΔH_{VL}	—	Enthalpy of vapor–liquid phase change, J/m² s
ΔH_{vap}	—	Heat of vaporization, J/kmol
δ	—	Thickness, m
ε	—	Porosity of the membrane
ϕ	—	Inclined angle
σ	—	Stefan–Boltzmann constant, W/m² K4
τ	—	Tortuosity of the membrane
τ_g	—	Effective heat penetration coefficient of glass

Superscripts

L	—	Liquid
V	—	Vapor

Subscripts

Air	—	Air
a	—	Ambient
aap	—	Ambient to absorption plate
ag	—	Ambient to glass
*ag*1	—	Air gap 1
*ag*2	—	Air gap 2
ap	—	Absorption plate
apg	—	Absorption plate to glass
g	—	Glass
ga	—	Glass to ambient
CL	—	Cold liquid
CONL	—	Condensing liquid
HL	—	Hot liquid
LF	—	Air gap 2-condensing liquid interface
ln	—	Logarithmic mean
*m*1	—	Hot fluid-membrane interface
*m*2	—	Membrane–air gap 2 interface
mem	—	Membrane
mp	—	Metal plate
*mp*1	—	Air gap 2–metal plate interface
*mp*2	—	Metal plate–cold fluid interface
ref	—	Reference
sys	—	System
water	—	Water

References

[1] D.R. Lloyd and K.W. Lawson, Membrane distillation, J. Membr. Sci., 124 (1997) 1–25.
[2] A.M. Alklaibi and N. Lior, Membrane-distillation desalination: status and potential, Desalination, 171 (2004) 111–131.
[3] M.S. El-Bourawi, Z. Ding, R. Ma and M. Khayet, A framework for better understanding membrane distillation separation process, J. Membr. Sci., 285 (2006) 4–29.
[4] S. Al Obaidani, E. Curcio, G. Di Profio and E. Drioli, The role of membrane distillation/crystallization technologies in the integrated membrane system for seawater desalination, Desal. Wat. Treat., 10 (2009) 210–219.
[5] K. Murase, Y. Yamagishi and K. Tano, Development of a hybrid solar distillator of a basin type distillator and a membrane distillator, Desal. Wat. Treat., 9 (2009) 96–104.
[6] F. Banat, N. Jwaied, M. Rommel, J. Koschikowski and M. Wieghaus, Performance evaluation of the "large SMADES" autonomous desalination solar-driven membrane distillation plant in Aqaba, Jordan. Desalination, 217 (2007) 17–28.
[7] F. Banat, N. Jwaied, M. Rommel, J. Koschikowski and M. Wieghaus, Desalination by a "compact SMADES" autonomous solar- powered membrane distillation unit, Desalination, 217 (2007) 29–37.
[8] J. van Medevoort, A. Jansen, J.H. Hanemaaijer, C. Dotremont, B. Nelemnas, E. van Sonsbeek, R. Biemans and H. Memstill Hylkema, Memstill: seawater desalination a solution to water scarcity, BMG–NMG Membrane Symposium. Antwerp, Belgium, November 16, 2008.
[9] H. Ben Bacha, M. Bouzguenda, T. Damak, M.S. Abid and A.Y. Maalej, A study of a water desalination station using the SMCEC technique: production optimization, Renewable Energy, 21 (2000) 523–536.
[10] L. Roca, M. Berenguel, L. Yebra and D.C. Alarcón, Preliminary modeling and control studies in AQUASOL project, Desalination, 222 (2008) 466–473.
[11] H. Chang, G.-B. Wang, Y.-H. Chen, C.-C. Li and C.-L. Chang, Modeling and optimization of a solar driven membrane distillation desalination system, Renewable Energy, 35 (2010) 2714–2722.
[12] H. Chang, J.-S. Liau, C.-D. Ho and W.-H. Wang, Simulation of membrane distillation modules for desalination by developing user's model on Aspen Plus platform, Desalination, 249 (2009) 380–387.
[13] K.G.T. Hollands, T.E. Unny, G.D. Raithby and L. Konicek, Free convective heat transfer across inclined air layers, J. Heat Transfer, 98 (1976) 189–193.
[14] W. Kays and M.E. Crawford, Convective Heat and Mass Transfer, 2nd ed., McGraw-Hill, New York, 1980, 127 p..
[15] S. Kakac, R.K. Shah and A.E. Bergles, Low Reynolds Number Flow Heat Exchangers, Hemisphere, Washington, D.C., 1983, 99 p.
[16] E.L. Cussler, Diffusion: Mass Transfer in Fluid Systems, 2nd ed., Cambridge University Press, Cambridge, UK, 1997, 178 p.
[17] E.N. Fuller, P.D. Schettler and J.C. Giddings, A new method for prediction of binary gas-phase diffusion coefficients, Indust. Eng. Chem. Res., 58 (1966) 18–27.
[18] A. Bejan, G. Tsatsaronis and M. Moran, Thermal Design and Optimization, John Wiley & Sons, New York, 1996.
[19] R.H. Myers and D.C. Montgomery, Response Surface Methodology: Process and Product Optimization using Designed Experiments, John Wiley & Sons, New York, 1995.
[20] M.D. McKay, R.J. Beckman and W.J. Conover, A comparison of three methods for selecting values of input variables in the analysis of output from a computer code, Technometrics, 22 (1979) 239–245.